

Title	Wirelessly Powered Sensing Fertilizer for Precision and Sustainable Agriculture
Author(s)	Kasuga, Takaaki; Mizui, Ami; Koga, Hirotaka et al.
Citation	Advanced Sustainable Systems. 2023, 2300314, p. 1-10
Version Type	VoR
URL	<a href="https://hdl.handle.net/11094/93236">https://hdl.handle.net/11094/93236</a>
rights	This article is licensed under a Creative Commons Attribution 4.0 International License.
Note	

***Osaka University Knowledge Archive : OUKA***

<https://ir.library.osaka-u.ac.jp/>

Osaka University

# Wirelessly Powered Sensing Fertilizer for Precision and Sustainable Agriculture

Takaaki Kasuga,\* Ami Mizui, Hirotaka Koga, and Masaya Nogi

Sensor networks comprising small wireless sensor devices facilitate the collection of environmental information and increase the efficiency of outdoor practices, including agriculture. However, the sensor-device installation density of a network is limited because conventional sensor devices must be removed after use. In this study, a sustainable dense sensing system that combines simplified degradable sensor devices, wireless power supply, and thermal-camera image-based information recognition is proposed. The proposed wireless-power-driven sensor device comprises a biodegradable nanopaper substrate, natural wax, and an eco-friendly tin conductive line. The sensor device emits a thermal signal based on the soil moisture content. The thermal camera simultaneously acquires the soil moisture-content data and sensor-device location. The majority of the sensor-device components are biodegradable, and the residual components have a minimal adverse impact on the environment. Additionally, the fertilizer component in the substrate promotes plant growth. The proposed sensing concept introduces a novel direction for realizing hyperdense sensor networks and contributes to the development of social systems that combine sustainability with meticulous environmental management.

production; this approach is commonly referred to as “precision agriculture.”<sup>[1–6]</sup> With the steady expansion of the global population and the associated surge in the demand for food, proficient crop cultivation using limited land and water resources is imperative. Precision agriculture is anticipated to be a viable solution to this problem.

Remote sensing technology plays an integral role in precision agriculture. Recently, the application of camera-equipped drones and satellite imagery has been increasingly adopted in agricultural production.<sup>[9,10]</sup> However, it is difficult to obtain certain information (such as humidity and soil moisture-content data) remotely; therefore, sensor devices must be installed at appropriate locations. The dense installation of sensor devices enables the collection of detailed information that accurately reflects the environment. The collected environmental information can then be

processed via machine learning and artificial intelligence;<sup>[11,12]</sup> note that a high volume of good quality data must be used as input to obtain accurate feedback.


However, the installation density of sensor devices is limited in terms of sustainability. A particular problem is the collection and disposal of used sensor devices. In previous studies, for example, large numbers of sensor devices were installed by scattering them from the air like plant seeds;<sup>[13–15]</sup> however, eventually, the sensor devices required collection because they were non-degradable. In other words, the recovery and disposal of sensor devices is a bottleneck that limits the density and scalability of feasible sensor networks.

Biodegradable material-based electronic elements and circuits have been developed to sustainably achieve mass production and consumption of sensor devices. Biodegradable electronics are being actively studied for medical, agricultural, and environmental monitoring applications, and various elements and devices have been proposed.<sup>[16–25]</sup> They are predominantly derived from proteins, polysaccharides, and biodegradable plastics. Research in this field is primarily related to single elements, such as sensors, and reports of electronic devices that combine multiple elements are limited.<sup>[22,23]</sup> This paucity is due to the difficulty in achieving compatibility between the required electronic device functions and the degradability of these devices. For sensor devices, sensing and data transmission functions are essential. In addition, sensing is meaningful only when linked to location

## 1. Introduction

The collection and analysis of environmental information is essential for all outdoor practices, including agriculture and environmental management. Recently, wireless communication sensor devices, which are diminutive and lightweight, have been adopted for environmental monitoring via sensor networks.<sup>[1–8]</sup> In agriculture, particular emphasis is placed on the utilization of sensor networks for gathering and employing environmental information (such as temperature, humidity, soil moisture content, and fertilizer concentration data) to enhance the efficacy of food

T. Kasuga, A. Mizui, H. Koga, M. Nogi  
SANKEN (The Institute of Scientific and Industrial Research)  
Osaka University  
8-1 Mihogaoka, Ibaraki, Osaka 567-0047, Japan  
E-mail: tkasuga@eco.sanken.osaka-u.ac.jp

 The ORCID identification number(s) for the author(s) of this article can be found under <https://doi.org/10.1002/adsu.202300314>

© 2023 The Authors. Advanced Sustainable Systems published by Wiley-VCH GmbH. This is an open access article under the terms of the Creative Commons Attribution License, which permits use, distribution and reproduction in any medium, provided the original work is properly cited.

DOI: 10.1002/adsu.202300314

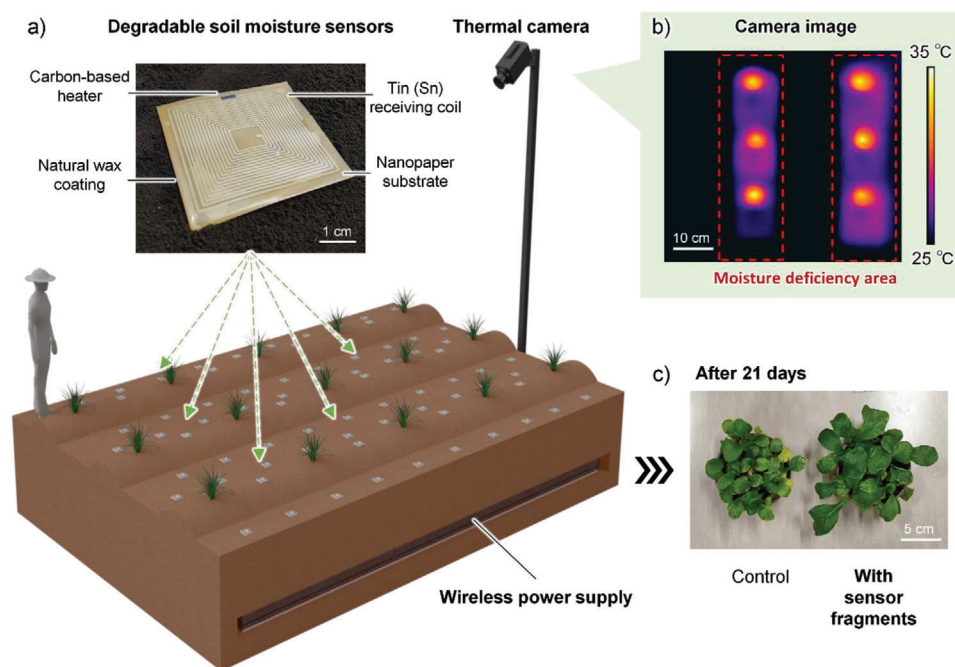


**Figure 1.** Proposed sensing system. a) Overview of the proposed sensing system with degradable sensor devices. b) When power is wirelessly supplied to the degradable sensor devices placed on the soil, the device heaters activate. The sensing location is determined from the hotspot location, and the temperature of the heater varies with the soil moisture content; thus, the soil moisture content is measured from the hotspot temperature. c) The degradable sensor devices are tilled into the soil after use. Subsequently, fertilizer components in the substrate of the sensor device are released into the soil, stimulating crop growth.

information. Owing to the difficulty in recording locations in advance when installing a large number of sensor devices in the environment, sensor devices must simultaneously transmit both sensing and location data. In other words, both sensing functionality and transmission of data, including location data, must be accomplished using a combination of only eco-friendly elements. To overcome these technical challenges, novel sensing systems are required.

Herein, we present a degradable sensor device and a novel concept for a high-density sensing system for sustainable and precision agriculture. To this end, we address the following two goals from all perspectives, including materials, circuit, and system design: 1) the majority of the sensor devices should be biodegradable and their residues should not adversely impact the environment and 2) the sensing and location data obtained by these devices should be remotely and simultaneously available.

## 2. Results

### 2.1. Proposed Sensing System

In this study, we focus on a soil moisture sensor, which is a crucial sensor in agriculture. The proposed sensing system comprises several degradable soil moisture sensor devices, a wireless power supply facility, and a thermal camera to acquire both sensing and location data (Figure 2). Each sensor device comprises a biodegradable paper substrate, a receiving coil composed of a tin (Sn)-printed conductive line, and a carbon-based heater. The sensor device is protected by a natural wax coating. The sensing system can be used as follows. First, a large number of sen-

sor devices are installed by scattering the devices across farmland, similar to how fertilizers are distributed (Figure 1a). Thereafter, the installed sensor devices receive power from their wireless power supplies, activating their heaters (Figure 1b). The efficiency of power transmission to the sensor device varies with the moisture content of the surface soil, and this power transmission efficiency is reflected in the temperature of the heater. Therefore, the soil moisture content can be determined using a thermal camera based on the detected hotspots (Figure 1b). As a hotspot corresponds to a sensor-device location, the sensing position is determined precisely based on the relative position of the camera and the ground surface.<sup>[26–28]</sup> Moreover, the sensor devices are composed of eco-friendly materials, most of which biodegrade in the environment, and the residual components are unlikely to adversely affect the environment. Following a certain period of usage (e.g., one season), the devices can be tilled into the soil. Once they are tilled, fertilizer components in the paper substrates are released into the soil and supply nutrients; thus, the sensor devices have a fertilizer application functionality (Figure 1c). Overall, a sustainable high-density sensing system is successfully achieved by combining a degradable sensor device, wireless power supply, and image-acquisition technology.

### 2.2. Selection of Eco-Friendly Conductive Materials

In this study, nanopaper was used as the sensor-device substrate. Nanopaper is a film composed of wood-derived cellulose nanofibers (CNFs) and has excellent properties, such as high strength, smooth surface, high heat resistance, and

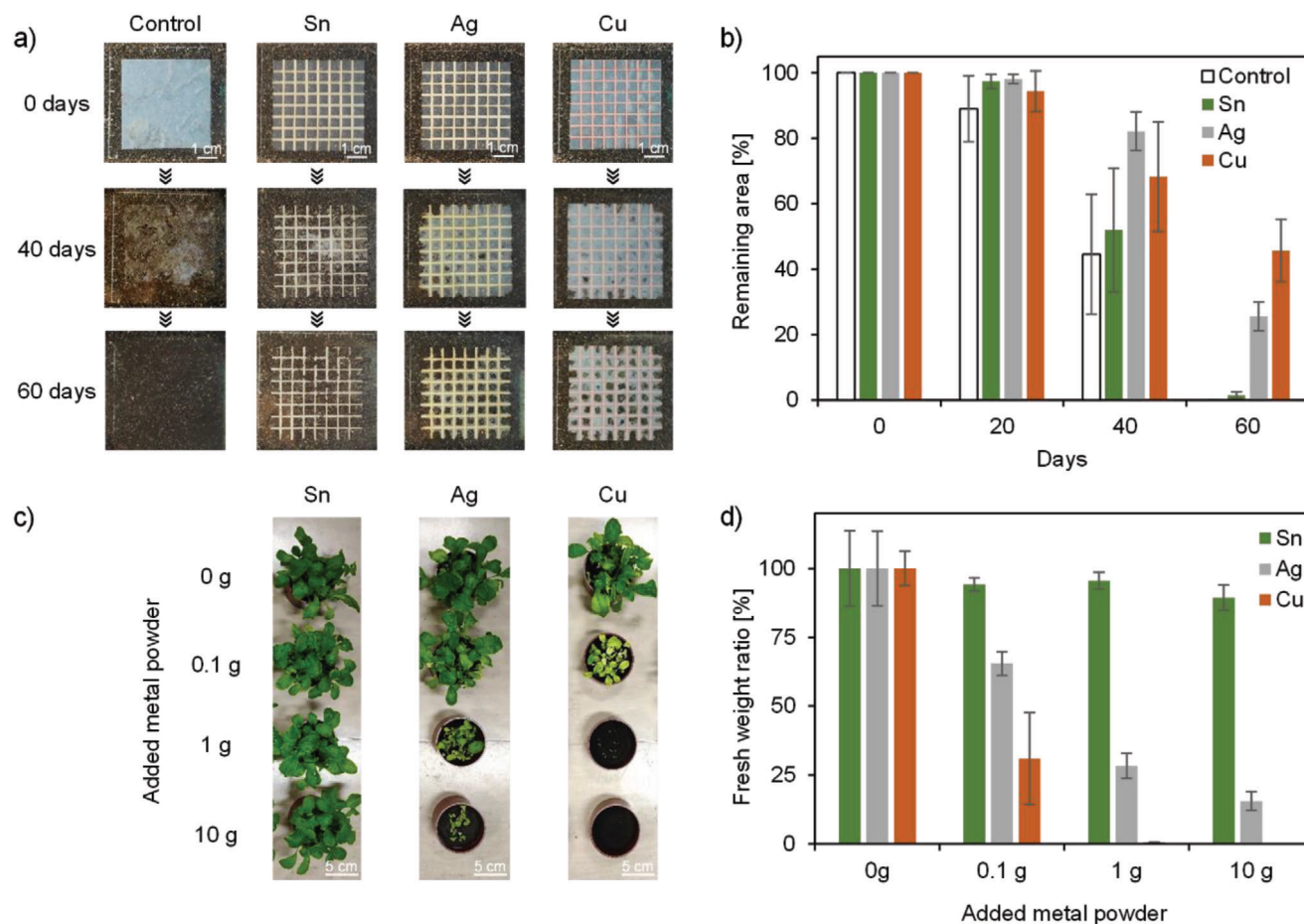


**Figure 2.** Biodegradation and plant cultivation tests. a) Biodegradation of nanopaper substrate (control) and nanopaper samples with tin (Sn), silver (Ag), and copper (Cu) lines. b) Nanopaper substrate with Sn lines biodegraded at the same rate as the control, but those with Ag and Cu lines biodegraded more slowly. c,d) Plant cultivation tests with Sn, Ag, and Cu powders in the soil (after 21 days). Cu caused significant plant damage even when present in small amounts. On the other hand, Sn does not cause significant plant damage even when present in the soil, unlike Ag and Cu.

biodegradability.<sup>[29–35]</sup> As nanopaper is composed entirely of plant fibers originating from the natural environment, special conditions are not required for biodegradation.<sup>[22,35]</sup> Indeed, nanopaper decomposes in the natural environment in the same manner as fallen leaves. For sensor devices that remain in the environment, a crucial consideration is the presence of metal components, such as conductive lines and electrodes. To date, no biodegradable material with sufficient conductivity has been reported. Therefore, in this study, three key factors are considered when selecting the conductive materials and fabrication methods to be used for the proposed sensor devices. The first factor is the effect on the substrate biodegradation. Ideally, sensor devices should rapidly degrade within a certain period after use, with unnecessary delays in biodegradation being undesirable. The second is the effect of the residual conductive lines on living organisms in the soil. The third factor is conductivity. Although the required conductivity depends on the circuit design, the volume resistivity of a conductive line to be used in sensor devices should be minimized to minimize energy consumption. Therefore, we focused on Sn as a conductive material. Sn is a metal with an atomic number of 50; it is soft and ductile, has a low melting point, and is stable and resistant to oxidation. Although Sn is not

typically used in conductive lines, inorganic Sn has poorer antibacterial properties than those of other common metals.<sup>[36,37]</sup> Moreover, Sn is not easily absorbed by plants and animals;<sup>[38,39]</sup> therefore, it is a suitable constituent material for degradable sensor devices.

Copper (Cu) and silver (Ag) are commonly used in sensor devices. Assuming a substrate composed of biodegradable materials, Cu and Ag lines were fabricated on different nanopaper samples and placed on natural soil. The biodegradation of the nanopaper substrates was then observed (Figure 2a). The biodegradation rates of the nanopaper substrates with Cu and Ag lines were significantly delayed compared to that of the control, which was a nanopaper substrate (Figure 2a,b). When Sn lines were mounted, the biodegradation rate was almost identical to that of the control. In soil, nanopaper is degraded by fungi and small isopods.<sup>[22,35]</sup> Thus, the differences in biodegradation rates observed for the samples in this test may have been caused by the differences in the antibacterial and biocidal properties of Cu, Ag, and Sn.<sup>[37]</sup>

Moreover, a plant cultivation test was conducted to simulate a scenario in which the metals remained in the soil. Test samples of komatsuna (*Brassica rapa var. perviridis*) were grown in pots, with

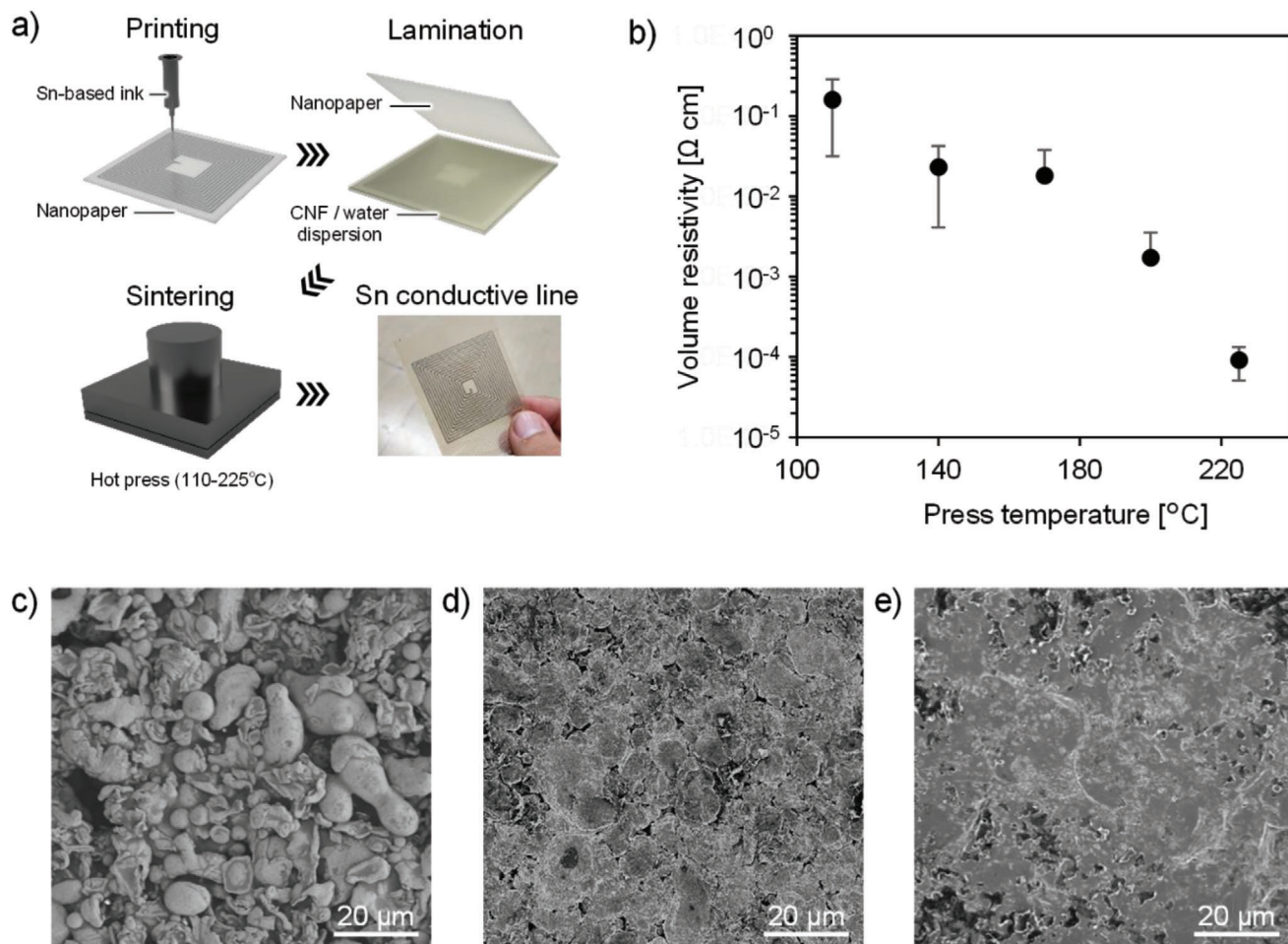


**Figure 3.** Fabrication of conductive lines. a) Processing steps for Sn conductive lines on nanopaper substrates. b) Owing to the high extensibility and low melting point of Sn, the volume resistivity of the Sn lines decreased with hot pressing at  $\approx 225^\circ\text{C}$ , which nanopaper substrates could withstand. Sn lines c) before and after hot pressing at d) 110 and e)  $225^\circ\text{C}$ . The Sn particles were well sintered by the hot pressing process.

0.1, 1, or 10 g of Cu, Ag, or Sn powder being added to each pot. The results confirm that the germination rates and growths degraded with higher contents of Cu or Ag powder (Figure 2c,d). The damage to plants caused by excess Cu or Ag ions is well documented.<sup>[40,41]</sup> Since the soil used in this study was acidic (pH 5.2), the Cu and Ag ions that leached from the conductive lines by the acidic soil may have inhibited the growth of the test sample. In contrast, no significant growth inhibition was observed for the Sn-containing samples, even for an excess amount of 10 g per pot (Figure 2c,d). Sn ions are not easily absorbed by plants,<sup>[38,39]</sup> which was confirmed by the results of the present study. Therefore, previous studies<sup>[38,39]</sup> and the above results suggest that Sn is a promising conductive material for eco-friendly sensor devices.

Sn conductive lines were fabricated via printing,<sup>[42–44]</sup> which has a low environmental impact and high productivity (Figure 3a). Ethanol ( $\text{C}_2\text{H}_6\text{O}$ )-solvent Sn ink was prepared by adding shellac, a biodegradable polymer, as a binder to Sn powder and adding ethyl cellulose for viscosity adjustment. The Sn ink was printed onto the nanopaper substrates using a dispenser. The conductivity of the Sn printed lines immediately

after printing was measured to be more than  $10^5$  [ $\Omega$  cm] and insulating (Figure 3b), primarily because the surface of the Sn powder was covered with a non-conductive Sn oxide layer<sup>[45,46]</sup> and numerous voids exist between the Sn powder particles (Figure 3c). To increase the conductivity, the Sn printed lines were sandwiched between nanopapers and hot-pressed at  $110^\circ\text{C}$ . The pressure deformation of the Sn particles reduced the inter-particle voids and the volume resistivity decreased to  $\approx 1.6 \times 10^{-1}$  [ $\Omega$  cm] (Figure 3b,d). When the temperature was further raised to  $225^\circ\text{C}$ , which is close to the melting point of Sn ( $232^\circ\text{C}$ ), the Sn particles were well sintered by heating and pressing and the volume resistivity decreased to  $9.2 \times 10^{-5}$  [ $\Omega$  cm] (Figure 3b,e). Press sintering is an established technique,<sup>[47–49]</sup> however, common biodegradable polymers, such as polylactic acid, soften at high temperatures<sup>[50]</sup> and maybe deformed during pressing. In contrast, the nanopaper substrate used in this study only showed a slight yellowing after a short hot press at  $225^\circ\text{C}$ . No deformation, rupturing, or pyrolysis, which would be problematic for application in a sensor device, occurred. Nanopaper has a high heat resistance, and CNF, of which nanopaper is composed, has no definite softening point at temperatures below  $250^\circ\text{C}$ .<sup>[51,52]</sup>

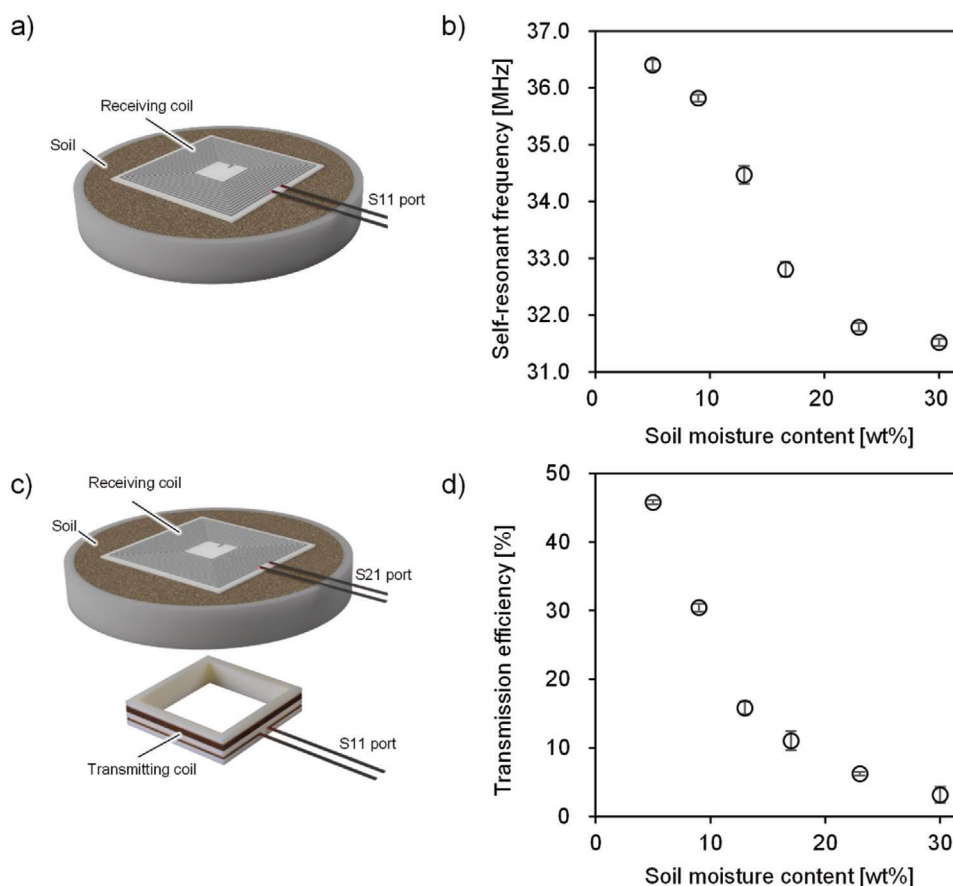


**Figure 4.** Wireless power supply. a) The self-resonant frequency of a receiving coil on soil was measured using a network analyzer. b) The self-resonant frequency of the receiving coil decreased as the soil moisture content increased. c) Transmitting and receiving coils were utilized to measure the power transmission efficiency. d) When a transmitter coil with a self-resonant frequency of 36.5 MHz was used, the power transmission efficiency maximized at 5% of the soil moisture content and decreased as the soil moisture content increased.

Overall, the prepared Sn-printed conductive lines sandwiched by nanopapers achieved excellent electrical conductivity of less than  $10^{-4}$  [ $\Omega$  cm] using a simple hot pressing technique.

### 2.3. Wireless Power Supply

We used wireless power via magnetic resonant coupling to supply power to the sensor device.<sup>[52–55]</sup> In the method, the transmission efficiency of the receiving coil is maximized when the transmitter and receiving coils are resonant. Thus, the power transmission efficiency depends on the degree of matching between the self-resonant frequencies of the transmitter and receiving coils.

A receiving coil was fabricated on a nanopaper substrate using Sn conductive lines. The self-resonant frequency of the receiving coil on the soil was measured using a network analyzer (Figure 4a). When placed on soil with 5% moisture content, the self-resonant frequency of the receiving coil mounted on the nanopaper substrate was  $\approx 36.5$  MHz (Figure 4b; Figure S1, Supporting Information). When placed on soil samples with different moisture contents, the self-resonant frequency of the receiving coil decreased as the soil moisture content increased (Figure

4b). Notably, this value decreased to  $\approx 31$  MHz when the receiving coil was placed on soil with 30% moisture content. The self-resonant frequency of the receiving coil was determined by the inductance and parasitic capacitance of the coil.<sup>[32,56]</sup> The parasitic capacitance of the coil was determined by the dielectric constant of the dielectric surrounding the coil. The dielectric constant of soil is known to vary with its moisture content;<sup>[57,58]</sup> therefore, the parasitic capacitance of the receiving coil was likely to change with the soil moisture content, yielding a change in the self-resonant frequency. Subsequently, a transmitter coil was placed 10 cm below the receiving coil and the transmission efficiency from the transmitter coil to the receiving coil was measured (Figure 4c,d). The self-resonant frequency of the transmitter coil was set to 36.5 MHz. Consequently, the transmission efficiency of a receiving coil installed on soil with 5% moisture content was  $\approx 46\%$  (Figure 4d; Figure S2, Supporting Information). The transmission efficiency decreased as the soil moisture content increased. Indeed, at 30% soil moisture content, the transmission efficiency decreased to  $\approx 3\%$  (Figure 4d; Figure S2, Supporting Information). This decrease in transmission efficiency can be attributed to a mismatch in the resonant frequency, and it was confirmed that the transmission efficiency varied with the

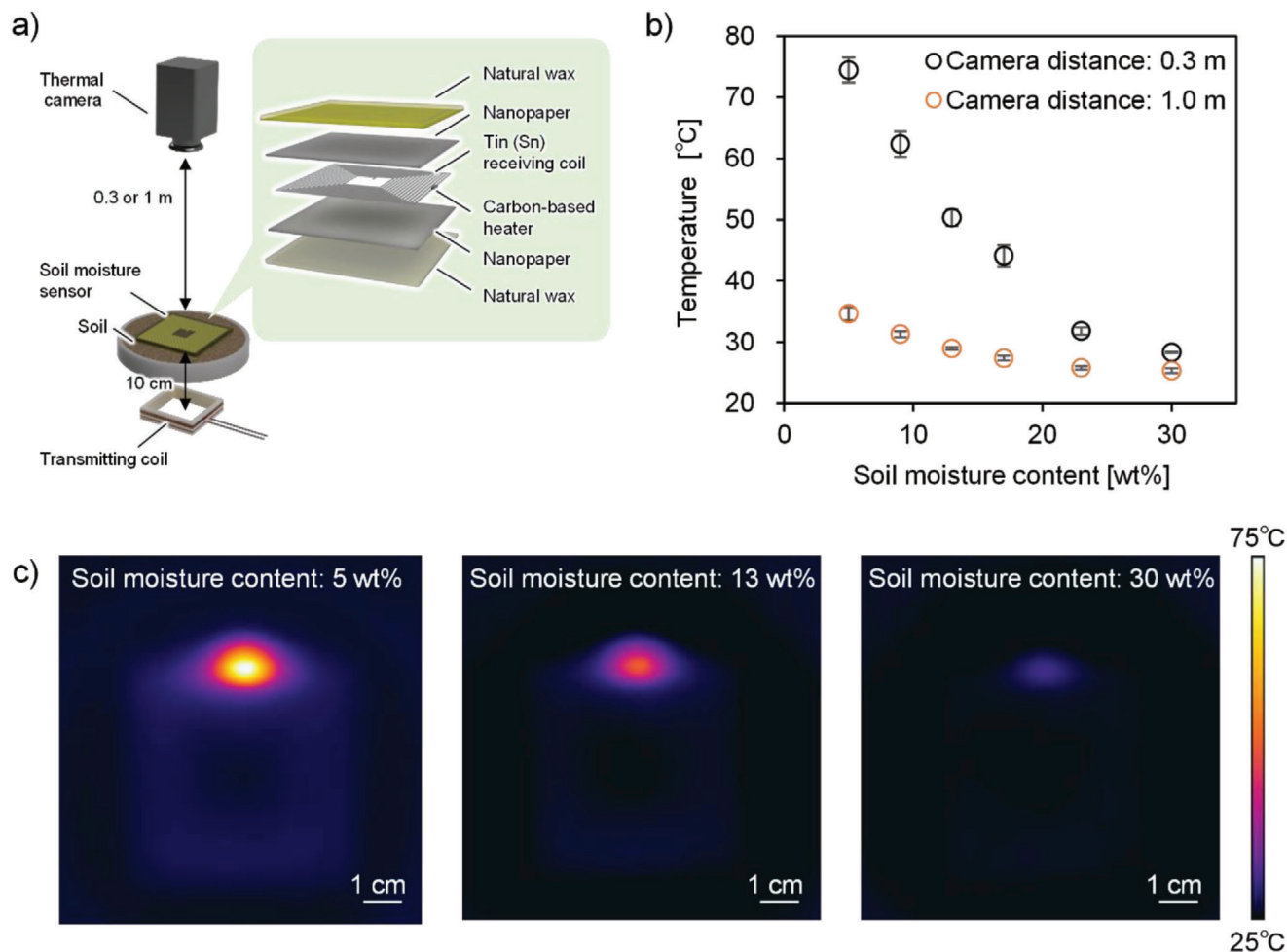


**Figure 5.** a) A wax-coated soil moisture sensor with a carbon-based heater, supplied with wireless power, was placed on the soil, and the heater temperature was measured using a thermal camera. b) During wireless power transmission, the heater temperature varied depending on the moisture content of the soil. c) The sensor device was observed using a thermal camera positioned 0.3 m above. The sensor-device location and the heater temperature linked with the soil moisture content observed as a hotspot.

moisture content of the soil in which the coil was installed. Note that these results were obtained in fixed positions and angles on smooth soil surfaces and may differ in practical situations.

#### 2.4. Hotspot Observation to Obtain Location and Soil Moisture Content

A carbon-based heater was used to externally transmit the change in the power transmission efficiency to the sensor device (Figure 5a; Video S1, Supporting Information). The power was supplied wirelessly from the transmitter coil (the self-resonant frequency of which was adjusted to 36.5 MHz) to the sensor device placed on the soil. When placed on soil with 5% moisture content, the heater element converted the received power into heat and heated to  $\approx 75$  °C after 1 min (Figure 5b,c). The heater temperature decreases as the soil moisture content increases (Figure 5b,c). Note that the heater element is small and, when the thermal camera is used from a distance, the temperature is averaged over the surrounding area; therefore, calibra-

tion may be required depending on the equipment and distance (Figure 5b). These results confirm that the developed sensor device is capable of transmitting changes in the surface-soil moisture content in the form of heater temperature.

#### 2.5. Demonstration

Various methods exist for obtaining location data, such as the Global Positioning System (GPS) and wireless beacons. However, using these methods, it is difficult to achieve the accuracy required for location data acquisition over medium distances in farmlands. Moreover, the complex device configurations required to implement these methods impair the overall sensor-device degradability, making it difficult to balance environmental considerations. Image recognition is a promising technology for simplifying sensor-device design and achieving the accuracy required for medium-range position acquisition.<sup>[26–28]</sup> The developed sensor device successfully transmitted the sensed soil moisture content to the outside environment via heat generation.

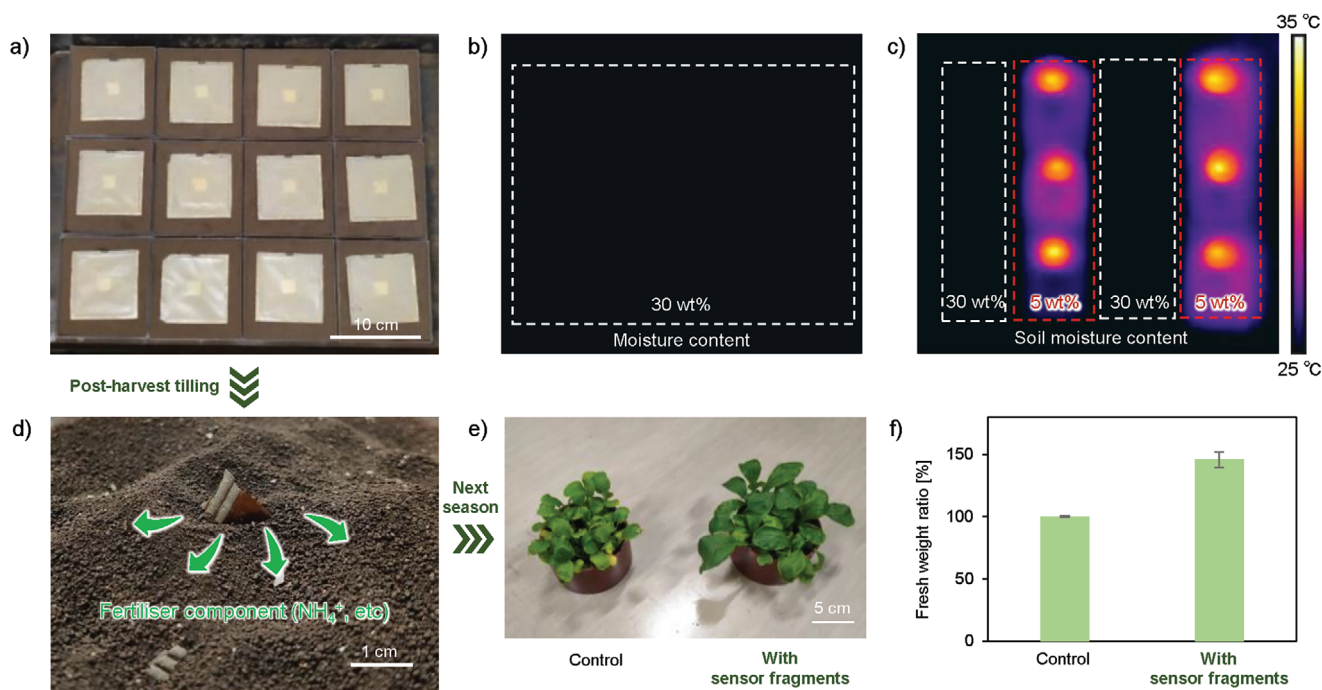


**Figure 6.** Demonstration of the proposed sensing system. a) Demonstration of high-density installation of degradable sensor devices. b) The resonant frequencies of the sensor devices and the transmitting coil did not match when the soil was sufficiently moist. No hotspots are identified. c) When some areas of the soil are dry, the sensor devices placed on the dry soil receive wireless power, the heaters generate heat, and hotspots are identified by the thermal camera. d) Used degradable sensor devices mixed into the soil, and e, f) the fertilizer components added to the nanopaper substrates promote plant growth.

Therefore, the sensor position and soil moisture content could be simultaneously determined from the heater temperature by observing the sensor-device installation position using a thermal camera. To demonstrate this concept, 12 moisture-content sensors were installed on a 0.4 m x 0.6 m field to map the soil moisture content (Figure 6a–c). A transmitting coil with a self-resonant frequency of 36.5 MHz was placed 10 cm below the field. The transmitter coil was a spiral coil that generated a uniform electromagnetic field over the field.<sup>[59]</sup> A thermal camera was placed 1 m above the field. When the soil moisture content was universally 30 wt.%, the sensor devices on the field generated little heat and the thermal camera did not detect any hotspots (Figure 6b). However, when some of the soil on the field was dry (moisture content: 5%), the sensor devices on the dry soil emitted thermal signals that were observed as hotspots in the thermal camera image (Figure 6c). This demonstration confirmed that the proposed novel sensing system enables the efficient acquisition of sensing data linked to location data, even when many sensor devices are densely installed.

As conventional sensor devices should be collected after use, it is difficult to install them at a high density because of the risk of leakage during collection and the problem of disposal after collection. The sensor device developed in this study is composed of biodegradable plant fibers and wax, Sn conductive lines, and carbon electrodes, which have a relatively minor environmental impact. Thus, most of the sensor device components are biodegradable and the residual components are unlikely to adversely affect agricultural crops. Coating sensor devices with natural waxes not only prevents moisture, but also reduces biodegra-

tion rates (Figures S3 and S4, Supporting Information). Coating materials such as natural waxes eventually biodegrade,<sup>[60–62]</sup> and it is crucial to consider the coating material selection and coating thickness depending on the set lifetime. It is not necessary to collect degradable sensors after use; therefore, they can be tilled with the soil following crop harvesting. Moreover, effective fertilizer application can be expected if fertilizer components are mixed into the nanopaper substrate, with the fertilizer components being released into the soil. As with general fertilizers, the duration and effectiveness of fertilizer application can be controlled by the fertilizer components blended into the substrate or wax. To demonstrate the sensing/fertilizer concept, we crushed sensor devices composed of nanopaper substrates containing a fertilizer component (ammonium sulfate,  $(\text{NH}_4)_2\text{SO}_4$ ) and mixed them with soil. A clear fertilizer application effect could be confirmed (Figure 6d–f). The nanopaper substrate can be compounded with a wide variety of fertilizer components and freely customized to suit the crops. Thus, the proposed concept is promising as a completely new type of high-density sensor device and sensing system that combines the mass installation of sensor devices while reducing the environmental impact.

### 3. Conclusion

In this study, we have proposed a novel sensing system tuned for high-density data collection and sustainability. The developed sensor device only consisted of plant fibers, eco-friendly conductive lines, natural wax, and carbon elements. Most of the device volume biodegrades in the environment and the remaining



conductive components have little adverse impact on the environment. The sensor device was powered by a magnetic resonant-coupled wireless power supply; it could transmit surface-soil moisture content data in the form of a temperature change. When images of the measurement area were captured using a thermal camera, the installation location and soil moisture content could be determined from the heat generation point and temperature.

The proposed system can be further developed, particularly in terms of the device configuration. In this study, sensor devices were placed at ideal positions and angles for wireless power transmission. In actual agricultural applications, it is not easy to keep the soil surface smooth, and the sensor device and power transmission system must be improved to accommodate uneven ground and changes in the angle from the transmitting coil. The Sn used as the wiring material in this study did not cause significant harm to the sample crop of *Brassica rapa var. perviridis*. It has been reported that Sn has no particular effect on many crops;<sup>[38,39]</sup> however, some crops are impacted by this substance. Fertilizers and pesticides are not completely free from side effects; therefore, careful consideration is required before their application. Similarly, degradable sensor devices must be optimized to suit the target crop and installation location. The development of eco-friendly conductive materials is crucial in the future. Although the simplest possible circuit and system were employed in this study, the circuit design and placement of the transmitting and receiving coils could also be improved to increase the resultant power transmission efficiency. Moreover, the need for a uniform power supply to support a large number of sensor devices is a potential obstacle in scaling up the proposed system. Therefore, a system that provides a uniform electric field over a wide area is required for the development of similar concepts.<sup>[63]</sup> In addition, further research is needed for cooperative operation with drones equipped with wireless power supply capabilities and for the use of microwave wireless power transmission<sup>[64]</sup> for operation in areas where there are no wireless power supply facilities. Finally, although the concept introduced in this study is based on agricultural applications, its use is not limited to that field. The application of the proposed system can be extended to the field of logistics in which large quantities of sensors are required, and to disaster areas where sensor device collection is difficult. Sensor devices and ultrahigh-density sensing systems with degradability, which is achieved by optimally simplifying their components, will contribute to the development of next-generation sensing systems, unrestricted by the existing bottlenecks.

## 4. Experimental Section

**Materials:** Acetic anhydride ((CH<sub>3</sub>CO)<sub>2</sub>O, purity: 99.9%), hydrogen peroxide (H<sub>2</sub>O<sub>2</sub>, purity: 35%), ethyl cellulose, potassium chloride (KCl, purity: 99.0%), (NH<sub>4</sub>)<sub>2</sub>SO<sub>4</sub> (purity: 99.5%), ethanol (C<sub>2</sub>H<sub>6</sub>O, purity: 99.5%), Ag powder (< 50 μm, purity: 99.99%), and graphite powder (purity: 99.0%) were purchased from Nacalai Tesque, Inc. (Japan). Cu powder (<50 μm, purity: 99.6%) was purchased from Hayashi Pure Chemical Ind., Ltd. (Japan). Sn powder (<50 μm, purity: 99.9%) was purchased from Kojundo Chemical Laboratory Co., Ltd. (Japan). Dewaxed shellac was purchased from Japan Shellac Industries, Ltd. (Japan). Carnauba and rice waxes were purchased from Yamakei Sangyo (Japan). Superphosphate of lime was purchased from Asahikogyo Co., Ltd. (Japan). Potting soil was purchased from Akagi Engei Co., Ltd. (Japan). Additionally, natural soil

was collected at 34°49'31.4''N 135°31'22.6''E and sieved through a 1 mm diameter mesh.

**Nanopaper Substrate:** To produce the nanopaper substrate, the pulp was first prepared by following the steps reported in a previous study.<sup>[22]</sup> Japanese cedar (*Cryptomeria japonica*) wood chips (60 g) were delignified in a (CH<sub>3</sub>CO)<sub>2</sub>O/H<sub>2</sub>O<sub>2</sub> mixture (500 mL/500 mL) at 90 °C for 2 h. The pulp slurry (≈3 wt.%) was then homogenized using a high-pressure waterjet system (Star Burst, HJP-25080; Sugino Machine Co., Ltd., Japan) equipped with an oblique-collision chamber. The injected slurry was repeatedly passed through a small nozzle (0.35 mm diameter) under 200 MPa pressure. After 10 passes through the nozzle, a 2.5 wt.% CNF/water dispersion was obtained. The CNF/water dispersion was cast evenly on an acrylic plate. Nanopapers with thicknesses of ≈40 μm were obtained after drying (PR-2 KT, ESPEC Corp., Japan) at 10 °C under 90% RH.

**Biodegradability and Plant Cultivation Test:** Biodegradability tests were performed according to the following procedure. Metal inks were prepared by mixing Cu, Ag, or Sn powders in a 5 wt.% ethyl cellulose/C<sub>2</sub>H<sub>6</sub>O solution. The ratio of each powder to the ethyl cellulose was 100:1. A mesh pattern with a 5 mm<sup>2</sup> aperture was drawn on a 40 mm × 40 mm nanopaper substrate using a dispenser (SHOTMASTER 200DS, MUSASHI Engineering, Inc., Japan). Nanopaper samples with metal lines were placed in 300 mL of natural soil in each pot. A glass plate was placed over the top to enable sample observation while replicating soil burial conditions. The soil moisture content was maintained at 30 wt.%, i.e., the moisture content of the soil when it was collected. The biodegradation tests were conducted at 25 °C for up to 60 d. The area of the remaining nanopaper substrate was calculated by analyzing a top-down image using ImageJ processing software.

Cultivation tests were performed according to previously reported methods.<sup>[65]</sup> Potting soils were mixed with KCl, (NH<sub>4</sub>)<sub>2</sub>SO<sub>4</sub>, and superphosphate of lime. A concentration of 100 mg of each of the active ingredients, (potassium (K), nitrogen (N), and phosphorus) was used per 500 mL of soil. Cu, Ag, and Sn powders were added to the test soils at doses of 0.1, 1, and 10 g per 500 mL. For the fertilizer efficacy test for fertilizer-containing soil moisture sensors, potting soil with no added fertilizer was used. One crushed sensor was used per 500 mL of soil. The soil moisture content was maintained at 45 wt.%. First, 500 mL of potting soil was placed in pots (113φ × 65 mm) without drainage holes; then, 20 seeds of komatsuna (*Brassica rapa var. perviridis*) were planted. The plants were grown for 21 days in an indoor constant-temperature room at 25 °C, 30% RH under LED lights for plant growth. After growth, the plants were harvested, and their fresh weights were measured. The fresh weight ratio was calculated, where the average fresh weight without metal powder addition was considered 100%. All soil moisture contents were measured using a moisture content meter (FD-800, Kett Electric Laboratory Co. Ltd., Japan) and adjusted using distilled water.

**Sn Conductive Lines:** Sn ink was prepared by mixing Sn powder with 5 wt.% ethyl cellulose/C<sub>2</sub>H<sub>6</sub>O and 50 wt.% shellac/C<sub>2</sub>H<sub>6</sub>O solutions. The ratio of Sn to ethyl cellulose to shellac is 100:1:1. Test electrodes (20 mm × 20 mm × 0.1 mm) were prepared by blade-coating the nanopapers with Sn ink. Once the C<sub>2</sub>H<sub>6</sub>O solvent was dried at room temperature, a thin layer of 2.5 wt.% CNF/water dispersion and another nanopaper substrate was applied to the first nanopaper substrate. The layers were then stacked in the following order: a PTFE plate, laminated nanopaper substrate, metal mesh, and paper towel. The layers were then pressed at 110 °C, 25 MPa for 10 min (AYS-R-5, Shinto Metal Industries, Ltd., Japan). The laminated nanopaper was then pressed at 110–225 °C, 25 MPa for ≈10 s to sinter the Sn particles. The thickness and the width of the Sn conductive lines were ≈0.1 and ≈1 mm, respectively.

**Sn Receiving Coil and Soil Moisture Sensor:** Receiving coils were fabricated using the same procedure as for the Sn conductive lines, for 65 mm × 65 mm spiral coils drawn using a dispenser. A probe coil was mounted around each receiving coil. A biodegradable hydrophobic coating was applied to the laminated nanopaper substrates with mounted receiving and probe coils by dipping them in carnauba wax heated to 100 °C. The self-resonant frequency (S<sub>11</sub>) was measured using a network analyzer (E5061A, Keysight Technologies, USA). The receiving coil was placed horizontally on soil with a moisture content of 5–30 wt.% (soil thickness:

30 mm). A Cu transmitter coil with a self-resonant frequency of 36.5 MHz and a probe coil was placed 10 cm directly below the receiving coil. The power transmission efficiency ( $|S_{21}|^2$ ) was then measured using a network analyzer. Each measurement was performed three times using a coil.

Thus, the soil moisture sensor consisted of a laminated nanopaper substrate on which a receiving coil, probe coil, and heater element were mounted and coated with carnauba wax. Carbon ink was prepared by mixing graphite powder with a 50 wt.% shellac/C<sub>2</sub>H<sub>6</sub>O solution. The ratio of graphite powder to shellac is 2:1. A 2 mm × 5 mm heater element was printed in connection with the probe coil via blade coating with carbon ink. Following printing, the C<sub>2</sub>H<sub>6</sub>O solvent was dried at room temperature. The weight of each sensor device was ≈2.6 g and contained ≈1.3 g of Sn. To prepare the soil moisture sensors with fertilizer, the same procedure was followed, where KCl and (NH<sub>4</sub>)<sub>2</sub>SO<sub>4</sub> were mixed to obtain 100 mg concentrations of each of the active ingredients (K and N) in the nanopaper substrate per sensor device. Each soil moisture sensor was placed on a 30 mm thick soil layer with a moisture content of 5–30 wt.%. Wireless power was supplied from a transmitter coil with a self-resonant frequency of 36.5 MHz placed 10 cm directly below the sensor. A 36.5 MHz signal was input to the transmitter coil using a function generator (FGX-295, TEXIO Technology Corporation, Japan) with a high-frequency amplifier (ZSA5151-10K250M, RAD Co., Ltd., Japan) having an output power of ≈6 W. The temperature of the heater element was measured using a thermal camera (FLIR ETS320, FLIR Systems, Inc., USA) that was positioned ≈0.3 or ≈1 m above the sensor. Each measurement was performed three times using a sensor device.

**Demonstration:** Twelve soil moisture sensors were placed on a 3 cm thick potting soil layer with 5 or 30 wt.% moisture content. These sensor devices were used from several sensor devices with comparable performance. A transmitter spiral coil with a self-resonant frequency of ≈36.5 MHz was placed 10 cm below the sensors. A 36.5 MHz signal was input to the spiral transmitter coil from a function generator via a high-frequency amplifier with an output of ≈50 W. The soil moisture content was mapped using a thermal camera positioned 1 m above the sensors.

## Supporting Information

Supporting Information is available from the Wiley Online Library or from the author.

## Acknowledgements

This work was partially supported by JST ACT-X (Grant Number JPMJAX21K3), Grants-in-Aid for Scientific Research (Grant Number 22K20592), Shorai Foundation for Science and Technology, and JST CREST (Grant Number JPMJCR22L3).

## Conflict of Interest

The authors declare no conflict of interest.

## Data Availability Statement

The data that support the findings of this study are available in the supplementary material of this article.

## Keywords

biodegradable sensors, cellulose nanofibers, nanocellulose, remote sensing, wireless power supply

Received: July 19, 2023  
Revised: September 21, 2023  
Published online:

- [1] N. Zhang, M. Wang, N. Wang, *Comput. Electron. Agric.* **2002**, *36*, 113.
- [2] I. F. Akyildiz, E. P. Stuntebeck, *Ad Hoc Netw.* **2006**, *4*, 669.
- [3] N. Wang, N. Zhang, M. Wang, *Comput. Electron. Agric.* **2006**, *50*, 1.
- [4] R. Gebbers, V. I. Adamchuk, *Science* **2010**, *327*, 828.
- [5] D. J. Mulla, *Biosyst. Eng.* **2013**, *114*, 358.
- [6] O. Elijah, T. A. Rahman, I. Orikumhi, C. Y. Leow, M. N. Hindia, *IEEE Internet Things J.* **2018**, *5*, 3758.
- [7] J. Yick, B. Mukherjee, D. Ghosal, *Comput. Netw.* **2008**, *52*, 2292.
- [8] A. Zanella, N. Bui, A. Castellani, L. Vangelista, M. Zorzi, *IEEE Internet Things J.* **2014**, *1*, 22.
- [9] C. Zhang, J. M. Kovacs, *Precis. Agric.* **2012**, *13*, 693.
- [10] J. S. Rawat, M. Kumar, *Egypt. J. Remote Sens. Sp. Sci.* **2015**, *18*, 77.
- [11] S. Wolfert, L. Ge, C. Verdouw, M.-J. Bogaardt, *Agric. Syst.* **2017**, *153*, 69.
- [12] A. Kamilaris, A. Kartakoullis, F. X. Prenafeta-Boldú, *Comput. Electron. Agric.* **2017**, *143*, 23.
- [13] P. Pounds, S. S. Singh in *IEEE Potentials*, Vol. 34, IEEE, New Jersey, USA **2015**, pp. 10–14.
- [14] B. H. Kim, K. Li, J.-T. Kim, Y. Park, H. Jang, X. Wang, Z. Xie, S. M. Won, H.-J. Yoon, G. Lee, W. J. Jang, K. H. Lee, T. S. Chung, Y. H. Jung, S. Y. Heo, Y. Lee, J. Kim, T. Cai, Y. Kim, P. Prasopsukh, Y. Yu, X. Yu, R. Avila, H. Luan, H. Song, F. Zhu, Y. Zhao, L. Chen, S. H. Han, J. Kim, et al., *Nature* **2021**, *597*, 503.
- [15] V. Iyer, H. Gaensbauer, T. L. Daniel, S. Gollakota, *Nature* **2022**, *603*, 427.
- [16] S.-W. Hwang, J.-K. Song, X. Huang, H. Cheng, S.-K. Kang, B. H. Kim, J.-H. Kim, S. Yu, Y. Huang, J. A. Rogers, *Adv. Mater.* **2014**, *26*, 3905.
- [17] G. Lee, S.-K. Kang, S. M. Won, P. Gutruf, Y. R. Jeong, J. Koo, S.-S. Lee, J. A. Rogers, J. S. Ha, *Adv. Energy Mater.* **2017**, *7*, 1700157.
- [18] G. A. Salvatore, J. Sülzle, F. Dalla Valle, G. Cantarella, F. Robotti, P. Jokic, S. Knobelspies, A. Daus, L. Büthe, L. Petti, N. Kirchgessner, R. Hopf, M. Magno, G. Tröster, *Adv. Funct. Mater.* **2017**, *27*, 1702390.
- [19] H. Jeong, S. Baek, S. Han, H. Jang, S. H. Kim, H. S. Lee, *Adv. Funct. Mater.* **2018**, *28*, 1704433.
- [20] H. Koga, K. Nagashima, Y. Huang, G. Zhang, C. Wang, T. Takahashi, A. Inoue, H. Yan, M. Kanai, Y. He, K. Uetani, M. Nogi, T. Yanagida, *ACS Appl. Mater. Interfaces* **2019**, *11*, 15044.
- [21] Y. Sui, M. Atreya, S. Dahal, A. Gopalakrishnan, R. Khosla, G. L. Whiting, *ACS Sustainable Chem. Eng.* **2021**, *9*, 2486.
- [22] T. Kasuga, H. Yagyu, K. Uetani, H. Koga, M. Nogi, *ACS Appl. Mater. Interfaces* **2019**, *11*, 43488.
- [23] J.-W. Shin, J. Chan Choe, J. H. Lee, W. B. Han, T.-M. Jang, G.-J. Ko, S. M. Yang, Y.-G. Kim, J. Joo, B. H. Lim, E. Park, S.-W. Hwang, *ACS Nano* **2021**, *15*, 19310.
- [24] H. Tao, S.-W. Hwang, B. Marelli, B. An, J. E. Moreau, M. Yang, M. A. Brenckle, S. Kim, D. L. Kaplan, J. A. Rogers, F. G. Omenetto, *Proc. Natl. Acad. Sci. USA* **2014**, *111*, 17385.
- [25] H. Yin, Y. Cao, B. Marelli, X. Zeng, A. J. Mason, C. Cao, *Adv. Mater.* **2021**, *33*, 2007764.
- [26] S. Manabe, C. Mouri, H. Tenzou, T. Kasuga, K. Motoki, *AIP Conf. Proc.* **2016**, *1733*, 020001.
- [27] A. Kampmann, M. Lamberti, N. Petrovic, S. Kowalewski, B. Alrifae, presented at IEEE Intell. Veh. Symp. Proc., IEEE, New Jersey, USA **2022**, pp. 1107–1113.
- [28] D. Horie, R. Katsuma, presented at IEEE 7th Ann. Comp. and Communication Workshop and Conf., IEEE, Las Vegas, NV, USA **2017**.
- [29] M.-C. Hsieh, C. Kim, M. Nogi, K. Suganuma, *Nanoscale* **2013**, *5*, 9289.
- [30] Y. Fujisaki, H. Koga, Y. Nakajima, M. Nakata, H. Tsuji, T. Yamamoto, T. Kurita, M. Nogi, N. Shimidzu, *Adv. Funct. Mater.* **2014**, *24*, 1657.
- [31] M. Nogi, M. Karakawa, N. Komoda, H. Yagyu, T. T. Nge, *Sci. Rep.* **2015**, *5*, 17254.
- [32] T. Inui, H. Koga, M. Nogi, N. Komoda, K. Suganuma, *Adv. Mater.* **2015**, *27*, 1112.

- [33] T. Kasuga, N. Isobe, H. Yagyu, H. Koga, M. Nogi, *Nanomaterials* **2018**, *8*, 104.
- [34] T. Kasuga, T. Saito, H. Koga, M. Nogi, *ACS Nano* **2022**, *16*, 18390.
- [35] U. Celano, K. Nagashima, H. Koga, M. Nogi, F. Zhuge, G. Meng, Y. He, J. De Boeck, M. Jurczak, W. Vandervorst, T. Yanagida, *NPG Asia Mater.* **2016**, *8*, e310.
- [36] H. Kawakami, K. Yoshida, Y. Nishida, Y. Kikuchi, Y. Sato, *ISIJ Int.* **2000**, *48*, 1299.
- [37] E. Zhang, X. Zhao, J. Hu, R. Wang, S. Fu, G. Qin, *Bioact. Mater.* **2021**, *6*, 2569.
- [38] K. A. Winship, *Acute Poisoning Rev.* **1988**, *7*, 19.
- [39] P. D. Howe, P. Watts, in *Tin and Inorganic Tin Compounds*, World Health Organization, Geneva **2005**.
- [40] A. R. Mir, J. Pichtel, S. Hayat, *BioMetals* **2021**, *34*, 737.
- [41] P. D. Howe, S. Dobson, in *Silver and Silver Compounds: Environmental Aspects*, World Health Organization, Geneva **2002**.
- [42] D. Tobjörk, R. Österbacka, *Adv. Mater.* **2011**, *23*, 1935.
- [43] R. V. K. Rao, K. V. Abhinav, P. S. Karthik, S. P. Singh, *RSC Adv.* **2015**, *5*, 77760.
- [44] Y. Khan, A. Thielens, S. Muin, J. Ting, C. Baumbauer, A. C. Arias, *Adv. Mater.* **2020**, *32*, 1905279.
- [45] S. Zhang, Y. Zhang, H. Wang, *J. Alloys Compd.* **2009**, *487*, 682.
- [46] J. Leitner, D. Sedmidubský, *J. Phase Equilibria Diffus.* **2019**, *40*, 10.
- [47] F. B. Swinkels, D. S. Wilkinson, E. Arzt, M. F. Ashby, *Acta Metall.* **1983**, *31*, 1829.
- [48] S. Akhtar, M. Saad, M. R. Misbah, M. C. Sati, *Mater. Today Proc* **2018**, *5*, 18649.
- [49] F. Wang, P. Mao, H. He, *Sci. Rep.* **2016**, *6*, 1.
- [50] C. Zhou, H. Guo, J. Li, S. Huang, H. Li, Y. Meng, D. Yu, J. De Claville Christiansen, S. Jiang, *RSC Adv.* **2016**, *6*, 113762.
- [51] H. Yagyu, S. Ifuku, M. Nogi, *Flex. Print. Electron.* **2017**, *2*, 014003.
- [52] M. Mariano, A. Dufresne, *ACS Symp. Ser.* **2017**, *1251*, 203.
- [53] A. Kurs, A. Karalis, R. Moffatt, J. D. Joannopoulos, P. Fisher, M. Soljac, *Science* **2007**, *317*, 83.
- [54] B. L. Cannon, J. F. Hoburg, D. D. Stancil, S. C. Goldstein, *IEEE Trans. Power Electron.* **2009**, *24*, 1819.
- [55] Z. Zhang, H. Pang, A. Georgiadis, C. Cecati, *IEEE Trans. Ind. Electron.* **2019**, *66*, 1044.
- [56] S. Shen, Z. Fan, J. Deng, X. Guo, L. Zhang, G. Liu, Q. Tan, J. Xiong, *Sensors* **2018**, *18*, 3022.
- [57] J. R. Wang, T. J. Schmutge, *IEEE Trans. Geosci. Remote Sens.* **1980**, *18*, 288.
- [58] Q. Chen, J. Liu, Z. Tang, J. Zeng, Y. Li, *IOP Conf. Ser.: Earth Environ. Sci.* **2014**, *17*, 012143.
- [59] K. Li, H. Zhao, Q. Liu, Y. Shi, C. Wang, P. Zhang, L. Wang, *Electr. Eng.* **2021**, *103*, 2009.
- [60] A. O. Hanstveit, *Chemosphere* **1992**, *25*, 605.
- [61] M. Irimia-Vladu, *Chem. Soc. Rev.* **2014**, *43*, 588.
- [62] M. Atreya, G. Marinick, C. Baumbauer, K. V. Dikshit, S. Liu, C. Bellerjeau, J. Nielson, S. Khorchidian, A. Palmgren, Y. Sui, R. Bardgett, D. Baumbauer, C. J. Bruns, J. C. Neff, A. C. Arias, G. L. Whiting, *ACS Appl. Electron. Mater.* **2022**, *4*, 4912.
- [63] T. Sasatani, A. P. Sample, Y. Kawahara, *Nat. Electron.* **2021**, *4*, 689.
- [64] M. A. Ullah, R. Keshavarz, M. Abolhasan, J. Lipman, K. P. Esselle, N. Shariati, *IEEE Access* **2022**, *10*, 17231.
- [65] K. Kawasaki, T. Kawasaki, H. Hirayasu, Y. Matsumoto, Y. Fujitani, *Sustain* **2020**, *12*, 4920.